Cylindrical crystal imaging spectrometer (CCIS) for cosmic x-ray spectroscopy.

Herbert W. Schnopper
Danish Space Research Institute, Lundtoftevej 7, DK-2800 Lyngby

and

Paul O. Taylor
Harvard-Smithsonian, Center for Astrophysics, 60 Garden Street
Cambridge, MA. 02138, USA

ABSTRACT

We have developed a "stigmatic" focusing, Bragg crystal spectrometer that has been used for high spectral resolution x-ray emission line diagnostics on hot laboratory plasmas. Our concept can be applied at the focal plane of an orbiting x-ray telescope where it offers several advantages over conventional spectrometers, i.e., mechanical simplicity, high resolving power and sensitivity, simultaneous measurement of an extended segment of spectrum, and good imaging properties. The instrument features a simple, unambiguous, non-scanning spectrum readout that is not adversely affected by either spacecraft pointing error or source extent. We estimate the performance of the instrument in the context of the Advanced X-Ray Astrophysical Facility (AXAF) mission.

I. INTRODUCTION

Careful interpretation of precise spectral information obtained by the x-ray spectrometers on the Einstein Observatory (1) has established the role of spectroscopy in the understanding of the underlying physical phenomena that drive many cosmic x-ray sources. The increased collecting area associated with the use of a grazing incidence reflection telescope on the Einstein x-ray observatory has allowed powerful spectroscopic techniques commonly used in other branches of physics to be applied to many of the stronger x-ray sources. Numerous cosmic x-ray emitters, including binary sources, supernova remnants, active galaxies and the intercluster gas have thermal components and many have been found to exhibit characteristic line emission. Fe line or edge structures have been observed, but with very low resolution (proportional counter), in several of the brightest sources. Emission lines from several highly ionized elements (among them O, Si, S) have been observed by the solid state (1) and focal plane crystal spectrometers (1) on the Einstein Observatory. The future need is for more precise and higher resolution data that can be interpreted within the context of a particular model to provide information on temperature, density, relative abundance, ionization equilibria, mass motion, redshift or particle size distribution. Previously, detector sensitivity was the prime consideration in astrophysical observations. For future missions higher resolution ($>10^2$) will be desirable and, in many instances required to make a choise between various conflicting models, to obtain line shapes for measuring temperature broadening and bulk gas motion, and to discriminate against spurious features from redshifted or satellite lines.

Much of the quantitative information contained in the spectrum can be obtained only from precise ratios of line intensities. The simultaneous recording of the He-like triplet and/or lines of H-like or Li-like series and their satellite lines, will reduce inaccuracies that could result from serial observations of fluctuating cosmic plasmas in the presence of a varying charged particle induced detector background. Parallel recording of all spectral features will aid in line identification and charge state analysis and will also improve the efficiency of finding features with unknown redshifts, absorbtion edges, and continuum levels.

We have developed a high wavelength resolution, "stigmatic" focusing, Bragg crystal spectrometer for line shape diagnostics of hot laboratory plasmas. The concept has been studied previously (2-4), but rarely applied in practice. It employs a cylindrically bent crystal (Fig. 1) to intercept x-rays that diverge with

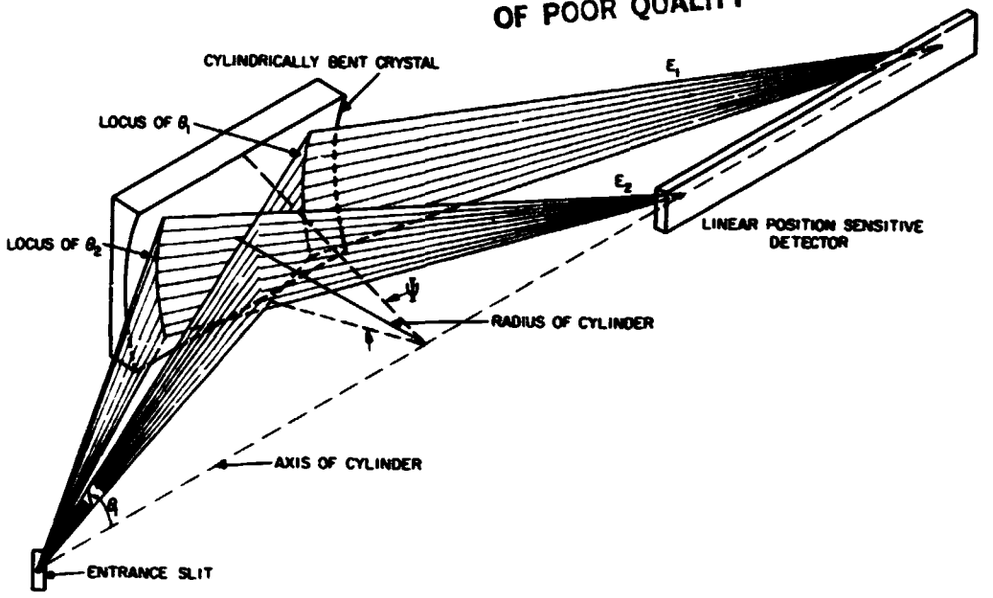

Fig. 1. CCIS concept; a cylindrical crystal surface gives exact point to point focus along the axis. Rays incident on the crystal at constant Bragg angle θ_1 define a conical surface about the axis with semi angle θ_1.

a broad range of Bragg angles θ from an entrance slit located on the axis of the cylinder. At each portion of the crystal those x-rays satisfying the local Bragg condition ($\lambda = 2d\sin\theta$, with d the lattice spacing) are reflected towards the axis where the dispersed spectrum is recorded on a position sensitive detector. This concept is to be contrasted with the more common Johann (5) design, cylindrical crystal spectrometer in which divergent x-rays are intercepted at almost constant Bragg angle. In the Johann design, a region of spectrum is scanned serially by changing the Bragg angle; hence, the relative position of focal point, crystal and detector must be adjusted repeatedly.

When the cylindrically curved imaging spectrometer (CCIS) is used at the focal plane of an x-ray telescope it can provide excellent imaging of an extended source. In the plane of the detector spatial information is displayed perpendicular to the cylinder axis while spectral information is displayed along the axis, and both can be recorded with a suitable two-dimensional, spatially resolving, detector. If, in some region of the spectrum, the predominent radiation is in an isolated narrow line, then then a two-dimensional image of an extended source will be recorded when the spectrometer is used without an entrance slit.

Finally, the unique focusing geometry of the cylindrical crystal makes it possible to exploit the greatly increased reflectivity of some mosaic crystals without a corresponding loss in resolution. With the inclusion of this benefit the cylindrically focusing spectrometer geometry will achieve a resolution and sensitivity equal to those of any current spectrometer design. In addition, the CCIS will have a large throughput since several hundred resolution elements are displayed simultaneously.

Our instrument has particular advantages for x-ray astronomy. The most important are:

1. An ability to measure simultaneously an extended segment of spectrum.
2. A spectrum integration mode in which scanning is unnecessary.
3. A simple unambiguous spectrum readout.
4. A minimal loss of energy resolution for extended or off-axis sources.
5. A high quality focus perpendicular to the dispersion plane.
6. A high resolving power, $E/\Delta E \gtrsim 10^2$.
7. A potential for increased sensitivity without loss of resolution if the high integrated reflectivity of mosaic crystals is exploited.
8. A geometry which does not require high resolution concentrating optics.

II. CCIS CONCEPT

A spectrometer concept in which the crystal is bent to a cylindrical surface that focuses and disperses the x-rays along the cylinder axis has been previously suggested (2,3) and its focusing properties and advantageous features have been examined in some detail (4).

The concept and geometry is illustrated in Figs. 1, 2, and 3. Rays from a point on the axis, incident on the cylindrically bent crystal at constant Bragg angle θ, define a conical surface about the cylinder axis with semi-angle θ (Fig. 1). We consider the crystal to be oriented at a central grazing angle θ_o with respect to the telescope axis about which the x-rays are diverging (Fig. 3).

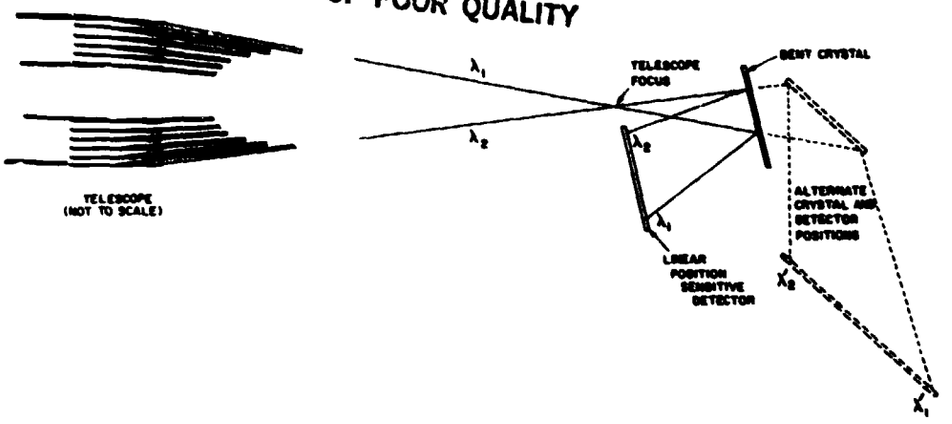

Fig. 2. CCIS at the focal plane of a grazing incidence telescope. Crystal and detector positions for two different wavelength bands are shown.

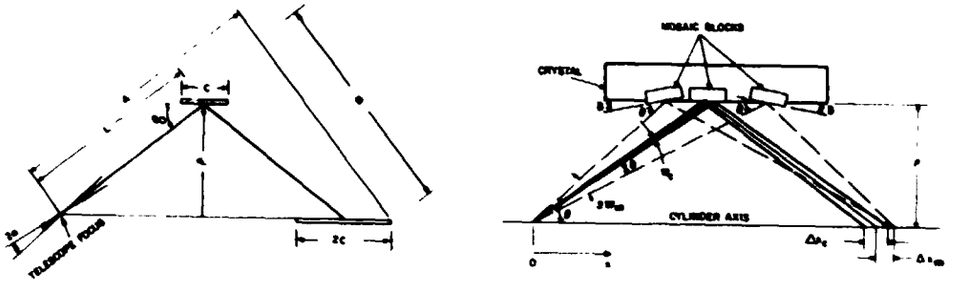

Fig. 3. Definition of spectrometer parameters.

Fig. 4. Effect of mosaic crystal structure on focus. Each block reflects over a range of angles W_c.

A. Wavelength dispersion.

X-rays of wavelength λ incident at Bragg angle θ are reflected in first order when $\lambda = 2d\sin\theta$, where d is the spacing of the diffracting crystal planes. If the crystal surface is a cylinder of revolution of radius ρ, rays originating on the cylinder axis are refocussed exactly onto that axis at a distance from the origin given by $x = 2\rho\cot\theta$. The wavelength dispersion along the x-axis is $\lambda = 2d/[1+(x/2\rho)^2]^{1/2}$ and the refocussed x-rays can be recorded by a linear, position sensitive, detector.

Relationships between detector spatial resolution x, angular resolution $\Delta\theta$, and energy ΔE, or wavelength resolution $\Delta\lambda$ are obtained by differentiating the expressions above. Thus,

$$dx = (2\rho/\sin^2\theta)d\theta \tag{1}$$

and

$$dE/E = d\lambda/\lambda = d\theta \cot\theta = (\sin 2\theta/4\rho)dx. \tag{2}$$

The crystal rocking curve width $\Delta\theta_c = W_c$ determines the limiting resolving power

$$S = (E/\Delta E)_c = \tan\theta/W_c, \tag{3}$$

and the corresponding limiting detector spatial resolution element

$$\Delta x_c = 4\rho/(S \sin 2\theta). \tag{4}$$

Several factors could degrade the angular or spectral resolution beyond the crystal limited value W_c and they have been analyzed in detail. Exact ray tracings indicate that no significant resolution loss will result from telescope aberations, pointing drift, or source extent.

The maximum telescope angular aperture 2α determines the crystal length C required to fully utilize that aperture (Fig.3);

$$C = \rho \sin 2\alpha/(\sin^2\theta_o - \sin^2\alpha) \simeq 2\alpha\rho/\sin^2\theta_o. \tag{5}$$

Assuming that there is a maximum convenient crystal size, then Eq. (5) sets an upper limit on ρ and on the other spectrometer parameters. The maximum fractional energy range which can be diffracted by one crystal at orientation θ_c is

$$(\Delta E/E)_\alpha \simeq 2\alpha \cot\theta_o, \tag{6}$$

which varies from 20% to 5% as θ_o is varied from 30° to 70°.

($2\alpha = 7^{o}$ for AXAF). This simultaneously diffracted energy band is sufficient to encompass the He-like triplet for all multiply charged ions (C to Fe) and, except for large θ_o, it also encompasses the H-like 2s - 2p/3p lines. When θ_o is reset to accommodate a specific energy band, the distance $L = \rho/\sin\theta_o$ (from slit to crystal, and from crystal to detector) must also be reset as is shown in Figs. 2 and 3. An instrument having L variable over nearly a factor of two and also having five or six interchangeable, cylindrically curved crystals available will accommodate the wavelength range from 25 Å to 1.5 Å, that covers all K lines and absorption edges from O to Fe.

B. Resolution

In this section we show that the spectral resolution of the cylindrical spectrometer is not significantly degraded by a mosaic crystal.

The probability $R(\theta,\lambda)$ of reflecting an x-ray of wavelength λ incident at an angle θ is sharply peaked about the Bragg angle. For a perfect crystal the full width at half maximum of this function is the single crystal diffraction width W_c. If the crystal is a mosaic of single crystal domains of appropriate microscopic size, then at each orientation of the crystal an x-ray can pass through many domains with slightly different orientations before being either absorbed or reflected. In this case, the "reflection window" or "half width" of the probability $R(\theta,\lambda)$ is the mosaic spread W_m which is generally larger than W_c.

Fig. 4 is a representation of this concept in the context of the cylindrical crystal geometry. A ray reflected at the Bragg angle from a mosaic block oriented parallel to the crystal surface will cross the crystal axis at a distance x given above. Rays of the same wavelength, however, incident on the surface at angles $\theta \pm \delta$, can reflect from mosaics tilted at angles $\pm \delta$ to the crystal surface, and will cross the axis at the distance

$$x = \rho\cot(\theta+\delta) + \rho\cot(\theta-\delta) \approx 2\rho\cot\theta\left[1+\delta^2/\sin^2\theta\right], \qquad (7)$$

which differs from the $\delta = 0$ position by

$$\Delta x_m - 2\rho\delta^2\cot\theta/\sin^2\theta. \tag{8}$$

The distribution of intensity in the image resulting from the mosaic effect is asymmetric with a peak at $x = 2\rho\cot\theta$ and a rapid fall-off towards larger x. Using $\delta = W_m$ as a measure of the resolution loss, we find that the mosaic broadening Δx_m, is equal to the single crystal diffraction limited resolution Δx_c given by Eq. (4) when

$$W_m = (W_c \tan\theta)^{1/2} = W_c S^{1/2} = \tan\theta/S^{-1/2}, \tag{9}$$

where S is given by Eq. (3). Mosaic spread orthogonal to the dispersion plane results in a large spatial blurring,

$$\Delta z_m = 2\rho\, W_m/(\sin\theta\cos\Psi), \tag{10}$$

where ψ is the half angle subtended by the crystal from a point on its axis (Fig. 1). An orthogonal tilt δ also results in a shift in Bragg angle of $\delta\theta = \delta^2\tan$. The associated spectral resolution loss will equal the diffraction limited value when

$$W_m = (2W_c\cot\theta)^{1/2} = 2S^{-1/2} \tag{11}$$

Thus, the maximum practical value for W_m is limited by Eq. (9) until $\tan\theta = 2^{1/2}$ and then by Eq. (11) and only if $W_m >> W_c$ will there be significant resolution loss resulting from the mosaic spread.

The efficiency of the spectrometer is, however, determined by the integrated reflectivity

$$R_c = \int_0^{\pi} R(\theta,\lambda)d\theta \tag{12}$$

which can be much greater for a mosaic crystal than a single crystal; roughly by the factor $W_m/W_c = S^{1/2}$.

Certain crystals can be prepared with domain structure that provides both a narrow diffraction width and a high integrated reflectivity. Two examples are graphite and lithium hydride which have theoretical single crystal resolving powers of ~ 5000 (2-5 keV) and ~ 0.5 to 1×10^5 (> 3.5 keV), respectively. Tolerable mosaic spreads are thus 0.8° for graphite at 2.5 keV and 0.4° for lithium hydride at 6.5 keV which are values typical of commercially available samples. Integrated reflectivities for ideal mosaic crystals are 18×10^{-4} for graphite and 35×10^{-4} for LiH; a factor of 10 or more higher than those for typical single crystals that might be chosen to reflect the same energy bands. This benefit of high integrated reflectivity together with high resolving power is not obtainable with scanning Bragg crystal spectrometers since, at each setting of the crystal, these instruments register on the detector the entire energy range determined by the rocking curve width W_m.

III. PERFORMANCE

A. Resolution

Design parameters for an instrument suitable for use at the focal plane of a large orbiting x-ray telescope are given in Table 1. Fig. 5 shows various spectrometer dimensions and Fig. 6 shows the resolving power limits imposed by telescope and spectrometer focusing and alignment aberrations. It is possible to have a very compact instrument without compromising on desired resolving power ($S \gtrsim 10^2$. If the spatial resolution of the detector is 0.2 mm x 3 mm it will impose a limiting spectral resolving power of S~4000 and a limiting transverse spatial resolution of 1 arcmin orthogonal to the dispersion plane. To accomodate the full range of Bragg angles ($2\alpha = 7^\circ$ and a field of view of 0.5°, the active area needs to be 20 cm x 10 cm (if $\rho = 20$ cm.).

TABLE 1

PARAMETERS OF AXAF TELESCOPE*

Effective area (wavelength dependent)	200-1000 cm^2
Pointing accuracy	± 30 arcsec
Aspect determination	± 1 arcsec
Focal length, F	10 m
Focal plane dispersion	50 m/arcsec
Focusing cone maximum angle, 2α	7
Resolution on axis	1 arcsec
7′ off axis	10 arcsec
15′ off axis	30 arcsec
20′ off axis	1 arcmin

PARAMETERS OF CYLINDRICALLY FOCUSING SPECTROMETER

Energy range, E	0.5 to 7.3 keV
Bragg angle range, θ_o	25^o to 70^o
Crystal length, C	100 mm
Crystal radius of curvature, ρ	200 mm
Detector pixel size	0.2 mm x 3 mm
Equivalent spatial resolution element	1 arcmin
Simultaneously recorded energy band $(\Delta E/E)_\alpha$	20% to 5%

*
These data are taken from AXAF Science Working Group Report, NASA TM-78285, May 1980.

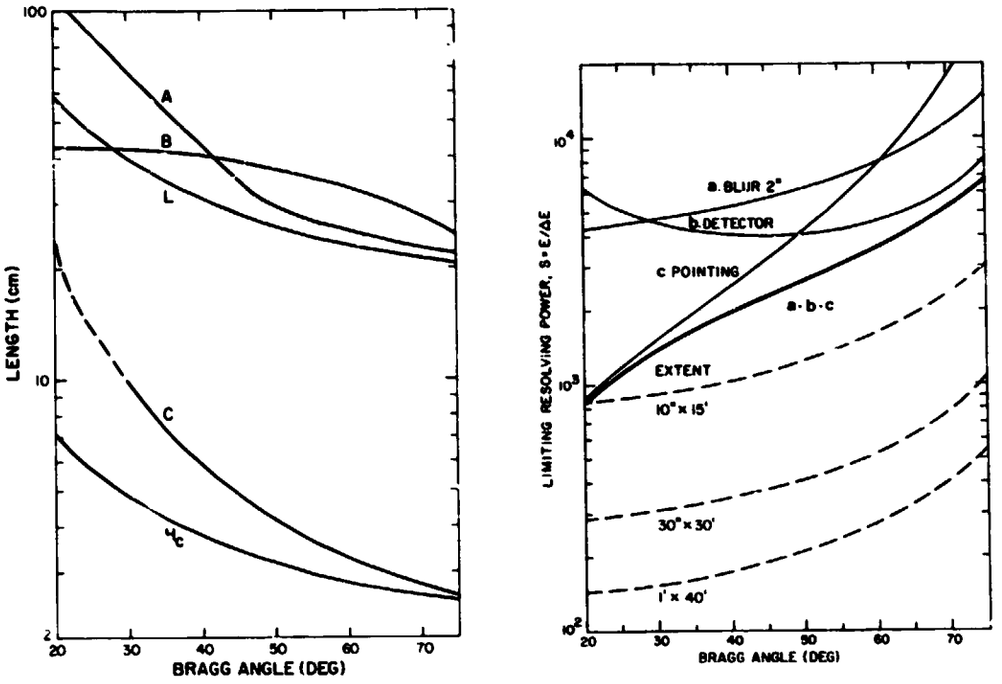

Fig. 5. Spectrometer dimensions corresponding to labels in Fig. 3: length A, bredth B, focal point to crystal distance L, minimum crystal length C, and crystal height H . All scale with the radius of curvature and have been computed for ρ = 200 mm.

Fig. 6. Spectral resolving power limits imposed by aspect drift (30 arcsec), telescope blur diameter (2 arcsec) and detector limiting spatial resolution (0.2 mm). The heavy curve combines these effects in quadrature and represents the geometric limit on resolving power for a point cosmic source. (Crystal resolving powers are shown in Fig. 7). The dashed curves show degraded resolving power due to source angular extent in the dispersion plane of 10 arcsec, 30 arcsec, 1 arcmin (corresponding to focal plane image widths of 0.5, 1.5 and 3 mm). Telescope blur diameter degrades approximately as the square of the off-axis angle and it is this effect, combined with abberations of the crystal focusing, which provided the indicated limits on source extent orthogonal to the dispersion plane.

Shown in Figs. 7 and 8 are resolving power and integrated reflectivities of several crystals (6-11) that can be used to cover the energy range from 0.5 to 7.3 keV. Spectrometer resolution can be limited by instrumental effects that must be combined with the crystal resolution. This is illustrated in the case of LiF (whose crystal resolving power is greater than 10^4) by showing in Fig. 7 the instrument resolving limit for a point cosmic source (from Fig. 6). The curves for ADP and RAP are similarly modified. When viewing an extended source a field of view of $1' \times 1^o$ will degrade the resolution to between 150 and 400.

B. Sensitivity

A spectral feature that contributes signal to a given detector pixel will be superimposed on an x-ray continuum (from bremsstrahlung, recombination, etc.) and a non x-ray background (from radiation belts, cosmic rays, etc). After an observing time t, the number of continuum photons recorded in a pixel of energy width ΔE_p from a point source contributing a flux $F_C(E)$ is

$$N_C = fF_C A_{eff} \Delta E_p t, \qquad (13)$$

where f is the fraction of the source imaged on the entrance slit and A_{eff} is the effective area $A_{eff} = (A/2\alpha)R_c \eta$ where $A/2\alpha$ is the average telescope collecting area per unit Bragg angle, and η is the proportional counter sensitivity. If n_b is non x-ray background count rate per detector pixel then the combined background is $N_B = N_C + n_b t$.

The response to a line of strength ($F_L \Delta E_L$) will be

$$N_L = f(F_L \Delta E_L) A_{eff} t/p. \qquad (14)$$

where it is assumed that the line covers p pixels. If the line is broad ($\Delta E_L >$ instrument resolution ΔE) then $p = \Delta E_L / \Delta E_p$; if the line is narrow $p = \Delta E / \Delta E_p$. The integrated line strength can be expressed in terms of the continuum, F_C and an equivalent line width, δE_L;

$$N_L = f(F_L \Delta E_L) A_{eff} t/p, \qquad (15)$$

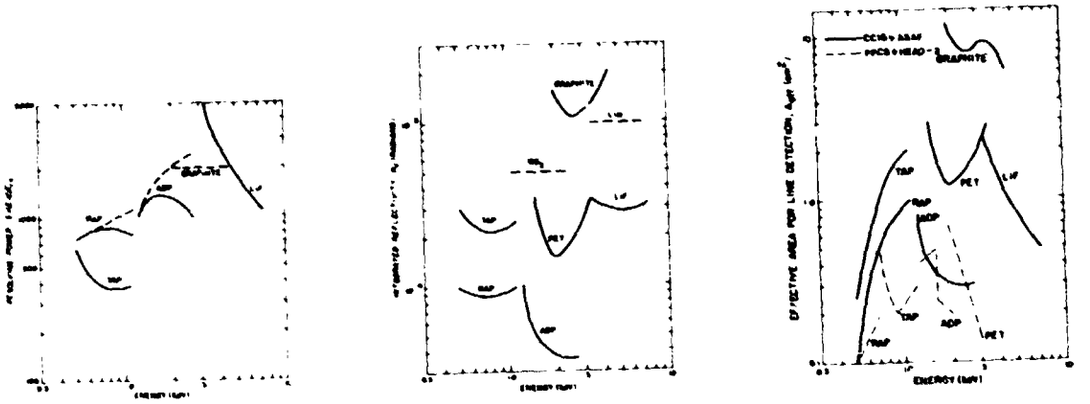

Fig. 7. Measured single crystal resolving powers for bendable crystals useful in the energy range 0.5 to 7 keV operating at Bragg angles $25^{o} < \theta_{o} < 70^{o}$. RAP TAP ; ADP (distorted crystal); Graphite ; LiF . In many cases the resolving power will be limited by instrumental effects (Fig. 6) as illustrated by the solid curves for LiF (whose crystal resolving power is greater than 10^{4}) ADP and RAP.

Fig. 8. Measured integrated reflectivities for crystal useful in the energy range 0.3 to 7 keV used at Bragg angles $25 < \theta_{o} < 70^{o}$. RAP, TAP, ADP ; PET ; LiF ; Graphite ; LiH, WS_2 (values for LiH and WS_2 are approximately one third the theoretical mosaic values).

Fig. 9. Expected effective detection areas, $A_{eff} = AR_{c}\eta/2\alpha$ for the proposed cylindrically focusing spectrometer at the focal plane of the AXAF. Effective area falls off at low energy due to proportional counter window transmission. For comparison equivalent effective areas for the HEAO-2 focal plane crystal spectrometer (FPCS) are shown (dashed curves).

If the line is detected in p channels, the minimum detectable number of counts signal $N_{L,m}$ can be written according to a 4σ criterion, $\rho N_{L,m}/\sigma(\rho N_{L,m}) = 4$, where $\sigma(\rho N_{L,m}) = \rho^{1/2}(N_{L,m}+N_B)^{1/2}$. It is assumed that the uncertainty in the background measurement is made negligible by sampling many background channels on either side of the line. Therefore for one channel

$$N_{L,m} = [8+(64+16\rho N_B)^{1/2}]/p \qquad (16)$$

The minimum detectable line flux is

$$F_L \Delta E_L = \rho N_{L,m}/(f A_{eff} t) \text{ photon cm}^{-2} \text{ s}^{-1}, \qquad (17)$$

and the minimum detectable equivalent width is

$$\delta E_{L,m} = \rho N_{L,m}/(f F_C A_{eff} t) \qquad (18)$$

The last quantity (a measure of signal to noise) is minimized by chosing p = 2 which is the smallest number of pixels consistent with proper sampling of the line width.

Sensitivities for three sample energies are calculated using the parameters listed in Table 2. We have set f = 1, p = 2, and used a $\Delta E_p < \Delta E = E/S$. Effective areas are shown in Fig. 9. They are used to calculate the minimum detectable line fluxes for a 1000 sec observation that are plotted in Fig. 10. Equivalent widths in keV can be obtained from the minimum fluxes by dividing by the corresponding continuum fluxes. The sensitivities are valid for line width $\Delta E_L < 2\Delta E_p$, but at low continuum flux levels (0.5 cm^{-2} s^{-1} keV^{-1}) the line sensitivity is signal limited and is valid for all line widths if the pixels are binned such that p = 2 effectively. For the Si line at ~ 2000 eV the gain in sensitivity using a mosaic graphite crystal versus a PET crystal is illustrated.

TABLE 2

PARAMETERS USED IN CALCULATING SPECTROMETER SENSITIVITIES

			FeXVII	SiXIII	SiXIV	FeXXV
Energy	E	(keV)	1.0	2.0	2.0	6.7
Disperser			TAP	PET	Graphite	LiF
Bragg Angle	θ_o	(deg)	28	45	67.5	27.5
Instrument Effective Area	A_{eff}	(cm^2)	1.8	1.2	12	0.5
Crystal Resolution	ΔE_c	(eV)	2.6	3*	1	<0.5
Instrument Resolution	ΔE	(eV)	2.6	3	1	6
Pixel Energy Width	ΔE_p	(eV)	1	1	1	3
Pixel Length		mm	1	0.4	0.6	0.4
Pixel Width**		mm	10	10	10	10
Background per pixel**	n_b	($10^{-4}s^{-1}$)	2.4	1.2	1.8	1
Simultaneous pixels	#		200	500	330	500
Extended Source Fraction	f		1			
Pixels per Line Width	p		2			
Radius of Curvature	ρ	mm	200			
Detector Length	2C	mm	200			

* Energy resolution for a mounted and vibrated PET crystal[7]; Best PET crystals show resolutions of 0.7 eV[7].

** The Einstein (HEAO-2) pixel area is about 1 cm^2 and backgrounds are scaled from reference 1.

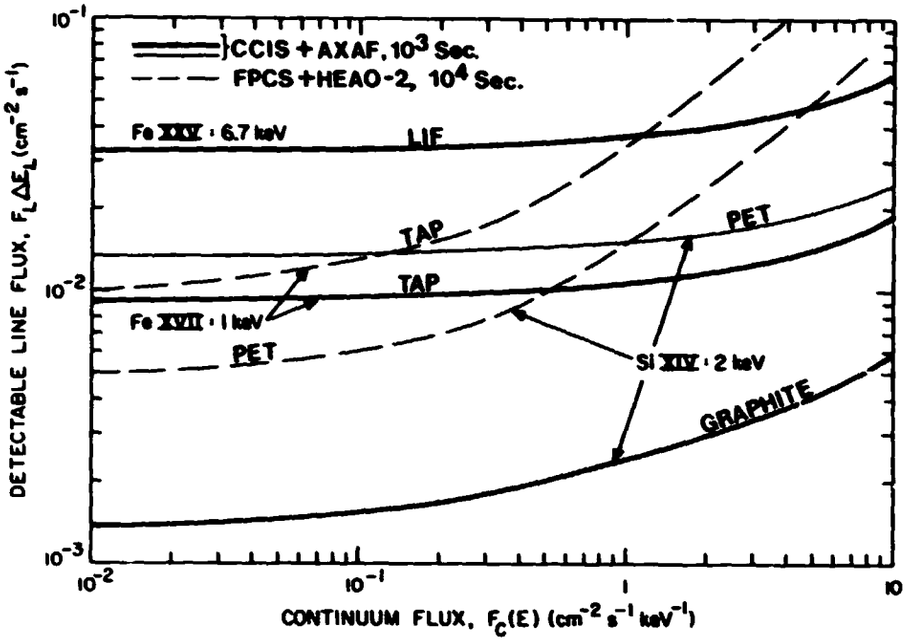

Fig. 10 Minimum detectable line fluxes at 4σ level for the proposed cylindrically focusing spectrometer at focal plane of AXAF (10^3 sec observation) and for the HEAO-2 focal plane crystal spectrometer (10^4 sec observation). These sensitivities can be compared directly since the AXAF telescope has about ten times the collection area of Einstein.

C. Comparison with Einstein Focal Plane Spectrometer.

Figs. 7 and 9 also show curves of resolving power and effective area for the Einstein focal plane spectrometer (12,13). The Einstein instrument suffers from severe focusing aberrations (12). It also has an order of magnitude worse resolution loss associated with drifting or extended sources and a more complicated spectrum readout. The crystal must be rocked and scanned during spectrum integration. CCIS, however, can achieve more uniform crystal limited resolving powers while still maintaining a large effective area per spectral resolution element. In Fig. 10 minimum detectable line fluxes for 10^4 sec Einstein observations are compared with our

predicted performance for a 10^3 sec observation with CCIS at the focus of the AXAF telescope. At 1 to 2 keV the AXAF telescope will have about 10 times the collection area of the Einstein telescope and, therefore, the curves may be taken as a comparison of the sensitivities of the two spectrometers. Thus, CCIS achieves comparable or better sensitivity per smaller resolution element while recording simultaneously several hundred channels of resolved spectrum thereby giving it a distinct throughput advantage.

IV. THE CONCEPT IN PRACTICE.

The components of a high resolution cylindrical focusing Bragg crystal spectrometer have been developed and fabricated. The instrument is currently operating at Alcator, the MIT tokamak, where it is used to obtain high quality, high resolution spectra emitted from the hot (approximately 2 keV) pulsed plasma. The instrument has a large (16.9 x 9.6 cm) PET crystal, (2d = 8.742 Å) bent to a radius of curvature of 60 cm, that is used at a Bragg angle of 34^o to diffract MoL radiation near 2500 eV (4Å) with a dispersion of $\sim$2 mÅ/mm. The energy range detected by the 250 mm long position sensitive proportional counter is 350 eV. The resolution of the system is limited by the present detector to a value of $E/\Delta E = 400$. Data acquisition and analysis is controlled by a minicomputer that provides a real time plasma diagnostic. Test spectra covering a 300 eV range from a Mo target x-ray tube have been recorded on film and they show the expected line widths for MoL lines (Fig. 11). Spectra have been recorded for several different plasma conditions at Alcator A. The main spectral features in the region around 2.5 keV are MoL x-ray emission and K emission from Helium-like Cl and S. A typical spectrum is shown in Fig. 12. The strong doublet at 4.4Å is the resonance line $2p \rightarrow 1s$ from Helium-like Cl and the broader feature is a superposition of emission lines from Mo 24^+ to 30^+.

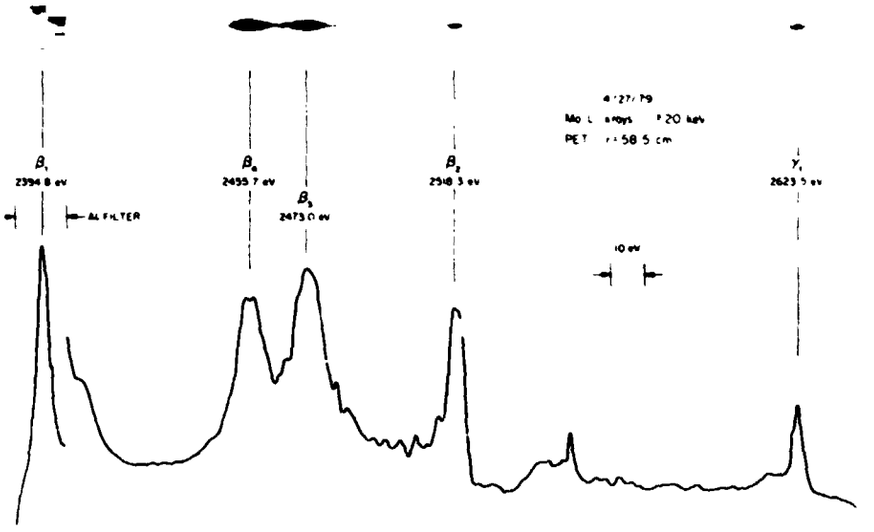

Fig. 11. Photographic plate and densitometer trace of a spectrum of a Mo target X-ray tube obtained with a cylindrically focusing spectrograph.

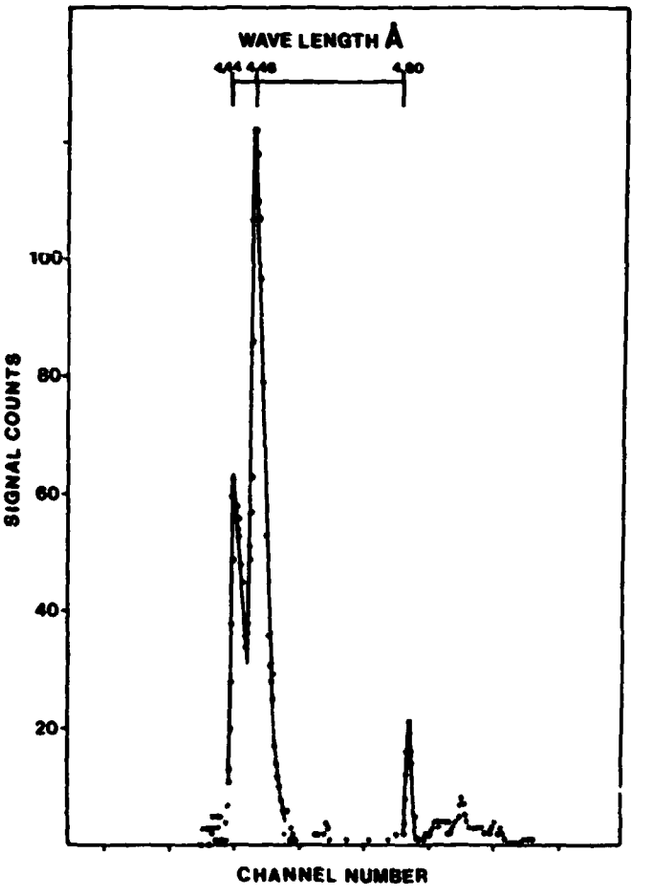

Fig. 12. Data from Alcator

Photographic spectra (14) have also been obtained with a smaller (ρ = 5 cm) spectrometer using mica to disperse x-rays emitted in the 10 - 11Å range from glass microballoons imploded by a two-beam Nd: Glass laser system at the University of Rochester, Laboratory for Laser Energetics. The results are shown in Figs. 13 and 14. Of particular importance is the trace orthogonal to the dispersion direction shown in Fig. 14. It illustrates the excellent spatial resolution by displaying the brightening of the target poles caused by the two incoming laser beams perpendicular to the cylinder axis.

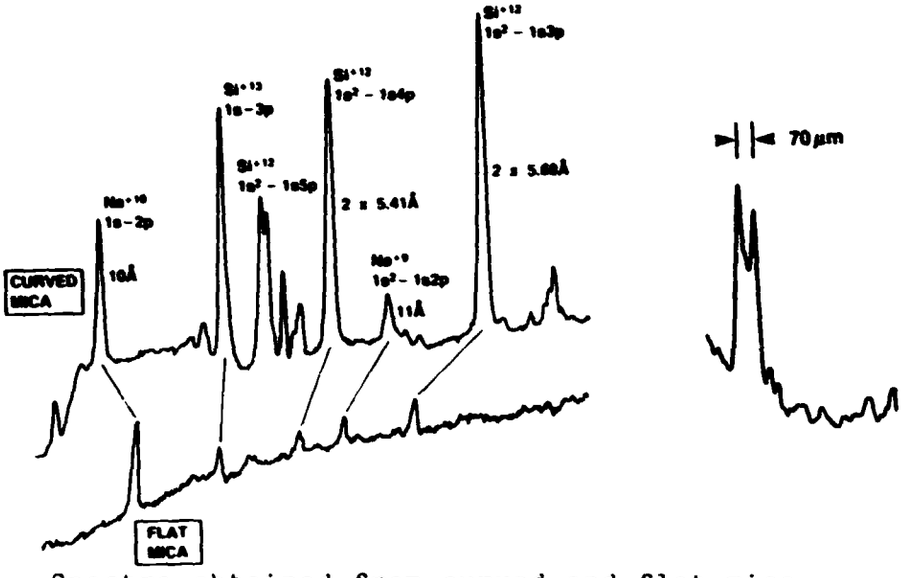

Fig. 13. Spectra obtained from curved and flat mica spectrographs. A comparison of collecting areas.

Fig.14 A trace orthogonal to the dispersion direction of a silicon line from a target of diameter 70μm.

These laboratory results show clearly the many advantages of the CCIS system and demonstrate its potential for cosmic x-ray spectroscopy.

V. CONCLUSIONS

The rich scientific yield from the spectrometer instruments carried by Einstein have emphasized the need to evaluate carefully the spectroscopic requirements of future missions. Throughput, spatial and spectral resolution, and wavelength range are variables in any combination of telescope focal plane spectrometer concept. For a given dispersing element

the question of throughput (i.e. sensitivity) is largely determined by the collecting area of the concentrating telescope. Resolutions, both spectral and spatial, are determined by the reflecting properties of the crystal and by the geometrical properties of the combined optical system. The upper limit on energy is usually set by the reflection efficiency of the telescope.

The dispersive spectroscopic systems on Einstein (transmission grating and Bragg spectrometer) require a high angular resolution telescope. As a result of the geometry of the optical system these instruments provide only modest spectral resolution and are almost totally ineffective when viewing extended sources. It is difficult to couple these instruments to any of the low resolution (1 arc min.) high throughput LAMAR systems without a severe degradation of performance.

The telescope/CCIS optical system is flexible with respect to both telescope resolution and source extent. In common with other good designs, CCIS will achieve crystal limited spectral resolution when it views the image of an on axis point source formed by a telescope having a high resolution. The distinguishing feature of CCIS is that it will achieve sufficient resolution to resolve the structure of the He-like emission structure when it views the image of an extended source formed by a telescope having only modest resolution and, in addition, it will provide simultaneously the intensity distribution across the source.

This work has been supported in part by the Smithsonian Institution and in part by the U.S. Department of Energy.

REFERENCES

1. R. Giacconi et al, Ap. J., 230, 540 (1979)

2. M. Guoy, Ann. Physique, 5, 241 (1916)

3. L. Van Hamos, Ann.d.Physik, 17, 716 (1933)

4. C.B. van der Berg and H. Brinkmam, Physica, 21, 85 (1955)

5. H.H. Johann, Z. Physik, 69, 185 (1931)

6. D.L. McKenzies, P.B. Landecker and J.H. Underwood, Space Sci. Instrum.,2, 125 (1976)

7. N.G. Alexandropoulos, Appl. Spectr., 28, 155 (1974)

8. J.P.R. Angel and M.C. Weisskopf, Ap. J., 75, 231 (1970)

9. D.B. Brown, M. Fatemi, and L.S. Birks, J. Appl. Phys., 45, 1544 (1974)

10. K.D. Evans, R. Hall, and M. Lewis, Space Sci. Instrum., 3, 163 (1977)

11. H.L. Kestenbaum, Appl. Spectr. , 27, 454 (1973)

12. H.W. Schnopper, J.P. Delvaille, A. Epstein, K. Kalata, and R. Sohval, Space Sci. Instrum., 2, 243 (1976)

13. C.R. Canizares, G.W. Clark, D. Bardas, and T. Market, SPIE, 106, 154 (1977)

14. B. Yaakobi, R.E. Turner, H.W. Schnopper, and P.O. Taylor, Rev. Sci. Instrum, 50, 1609 (1979)